Rapid increases in shrubland and forest intrinsic water-use efficiency during an ongoing megadrought

Steven A. Kannenberg[a,1,2], Avery W. Driscoll[a,2], Paul Szejner[b,c], William R. L. Anderegg[a], and James R. Ehleringer[a]

[a]School of Biological Sciences, University of Utah, Salt Lake City, UT 84112; [b]Instituto de Geología, Universidad Nacional Autónoma de México, 04510 Mexico City, Mexico; and [c]Laboratory of Tree-Ring Research, University of Arizona, Tucson, AZ 85721

Edited by Susan Trumbore, Max Planck Institute for Biogeochemistry, Jena, Germany; received September 30, 2021; accepted November 11, 2021

Globally, intrinsic water-use efficiency (iWUE) has risen dramatically over the past century in concert with increases in atmospheric CO_2 concentration. This increase could be further accelerated by long-term drought events, such as the ongoing multidecadal "megadrought" in the American Southwest. However, direct measurements of iWUE in this region are rare and largely constrained to trees, which may bias estimates of iWUE trends toward more mesic, high elevation areas and neglect the responses of other key plant functional types such as shrubs that are dominant across much of the region. Here, we found evidence that iWUE is increasing in the Southwest at one of the fastest rates documented due to the recent drying trend. These increases were particularly large across three common shrub species, which had a greater iWUE sensitivity to aridity than *Pinus ponderosa*, a common tree species in the western United States. The sensitivity of both shrub and tree iWUE to variability in atmospheric aridity exceeded their sensitivity to increasing atmospheric [CO_2]. The shift to more water-efficient vegetation would be, all else being equal, a net positive for plant health. However, ongoing trends toward lower plant density, diminished growth, and increasing vegetation mortality across the Southwest indicate that this increase in iWUE is unlikely to offset the negative impacts of aridification.

climate change | drought | iWUE | stable isotopes | tree rings

Plant stomata are the apertures that control the exchange of CO_2 and water vapor between the leaf and atmosphere and are thus inextricably linked to carbon (C) and water cycles at local to global scales (1–4). Intrinsic water-use efficiency (iWUE), the ratio of photosynthesis (A) to stomatal conductance (g_s), serves as an indicator of stomatal responses to environmental variability and is indicative of the tradeoff between C uptake and water loss. Globally, iWUE has increased sharply over the last century, largely due to increases in atmospheric CO_2 concentration allowing plants to increase A and/or decrease g_s (5–7). Water availability is another primary factor determining iWUE, as plants may open stomata when water is plentiful and close them when water is scarce. Indeed, evidence from atmospheric isotope ratios and upscaled flux data has shown that the impacts of drought on iWUE are detectable at continental scales (8, 9). Ongoing increases in the frequency and severity of drought in many regions of the world (10) are thus expected to accelerate the ongoing increases in iWUE due to rising [CO_2]. However, the sensitivity of iWUE to drought is highly variable across species, and understanding this variability is a crucial challenge for predicting vegetation responses to climate change.

The American Southwest is currently in the grips of a large-scale "megadrought," one of the most serious multidecadal drought events in the region over the last 1,200 y (11). The impacts of this drought have been acutely felt by vegetation, with evidence pointing to widespread reductions in C uptake (12), cumulative stress impacts (13, 14), and severe drought-induced dieback events in recent decades (15–18). Unfortunately, direct measurements of iWUE that capture this drought are rare and largely constrained to tree-ring chronologies. Tree-ring chronologies are traditionally the primary method for discerning long-term iWUE trends since a single sampling can produce a time series of iWUE over the lifespan of the tree. However, this approach likely biases estimates of Southwestern iWUE trends toward the region's more mesic high elevation forests, which differ greatly in vegetation composition and climate as compared to the lower elevation desert ecosystems that also characterize the region. Moreover, iWUE estimates from trees are likely not indicative of other key plant functional types such as shrublands, which constitute a vast area of the Southwest (Fig. 1*A*). Thus, in addition to occupying distinct climatic zones (*SI Appendix*, Fig. S1), iWUE derived from tree rings may not capture the different sensitivities of other plant functional types to [CO_2] and aridity (19). As aridification in the Southwest is expected to continue into the future (20–22), quantifying trajectories in iWUE across functional types is crucial to understand the acclimation and adaptive responses of vegetation across the landscape and to project changes to C and water cycles.

While long-term iWUE records are rare in nontree plant functional types, a recent study showed that shrub populations in the Southwest have increased iWUE faster than most forests globally (24). It remains unknown, though, if this rapid rate of increase in iWUE is due to a greater sensitivity of shrubs than trees to aridity and [CO_2], the ongoing aridification trend, or both. A rigorous understanding of future vegetation physiology and ecosystem carbon/water cycling hinges on disentangling the

Significance

Photosynthesis involves a tradeoff between the uptake of carbon and the loss of water. Intrinsic water-use efficiency is an indicator of this tradeoff that is pivotal for understanding plant responses to climate change. Global increases in atmospheric CO_2 concentration have increased intrinsic water-use efficiency, but this relationship is also modulated by water availability. Here, we have identified that a severe, multidecadal drought in the American Southwest has caused some of the largest increases in plant water-use efficiency ever observed. The increase was particularly large in shrubs, which dominate much of the landscape in the region. Given that water scarcity in the American Southwest is expected to worsen, these relationships have important implications for plant health and carbon and water cycling.

Author contributions: S.A.K., A.W.D., P.S., and J.R.E. designed research; S.A.K., A.W.D., P.S., and J.R.E. performed research; S.A.K., A.W.D., and W.R.L.A. contributed new reagents/analytic tools; S.A.K. and A.W.D. analyzed data; and S.A.K., A.W.D., P.S., W.R.L.A., and J.R.E. wrote the paper.

The authors declare no competing interest.

This article is a PNAS Direct Submission.

[1]To whom correspondence may be addressed. Email: s.kannenberg@utah.edu.

[2]S.A.K. and A.W.D. contributed equally to this work.

This article contains supporting information online at http://www.pnas.org/lookup/suppl/doi:10.1073/pnas.2118052118/-/DCSupplemental.

Published December 20, 2021.

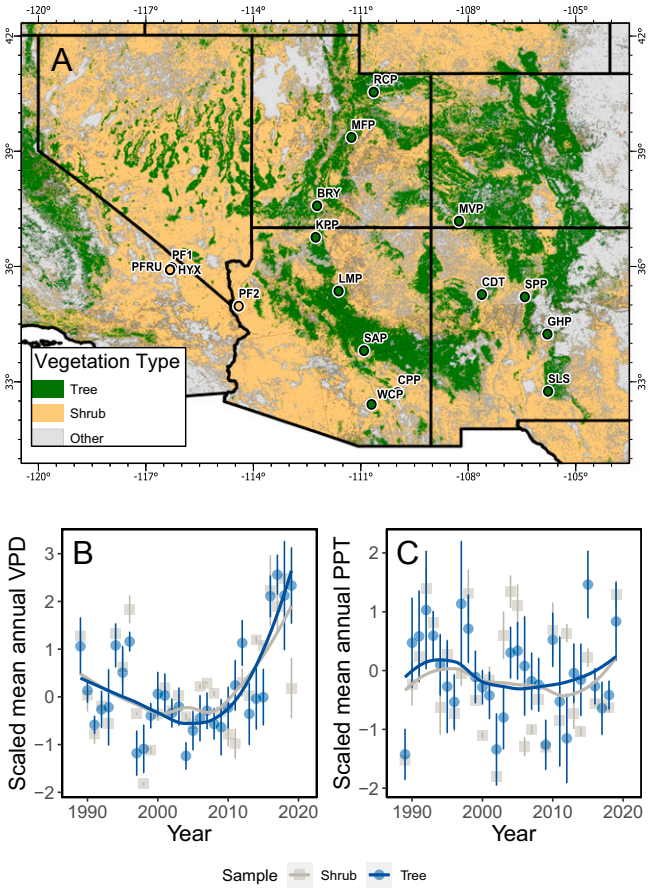

Fig. 1. Map of study sites and rates of recent climate change at all sampled sites. (*A*) Study sites with associated land cover representing shrub or tree dominated landscape (Table S1), classified via LANDFIRE (23). (*B*) Scaled annual maximum VPD and (*C*) scaled mean annual PPT across sites. Black lines in *A* represent state lines. Points in *B* and *C* represent means ± SD for each sample type (shrub versus tree), and smoothing lines represent a loess regression with a span of 0.5.

climatic versus physiological controls on iWUE. Here, we leverage a spatially and temporally extensive dataset of plant iWUE as derived from $\delta^{13}C$, spanning three decades of annual measurements across four shrub populations and 13 *Pinus ponderosa* stands, a dominant and widespread conifer species in the region (*SI Appendix*, Table S1). We sought to test the hypotheses that 1) the rapid increase in iWUE in the American Southwest is linked to the ongoing megadrought and 2) iWUE in shrubs is more sensitive to this aridification than in *P. ponderosa* due to a greater innate sensitivity of this plant functional type.

Results and Discussion

Recent Changes in Climate and iWUE. The ongoing megadrought has impacted the climate of the American Southwest over the study period. Since 1989, mean annual vapor pressure deficit (VPD) significantly increased at 9 out of 17 sites (Fig. 1 *B* and *C* and *SI Appendix*, Table S2). However, the rate of increase in VPD has accelerated over sevenfold in the past decade, resulting in significant increases in VPD since 2010 at 14 sites. This aridification was largely the result of increasing VPD, as there were no detectable changes in annual mean precipitation (PPT) over the past three decades at any site. Over this period, iWUE increased drastically across sites and species (Fig. 2 and *SI Appendix*, Table S3). Earlywood iWUE increased by 0.79 ± 0.007 (SE) μmol CO_2 mol H_2O^{-1} yr^{-1}, latewood iWUE increased by 0.70 ± 0.009 μmol CO_2 mol H_2O^{-1} yr^{-1}, and shrub foliar iWUE increased by 1.04 ± 0.18 μmol CO_2 mol H_2O^{-1} yr^{-1}, though there was substantial variability between sites (*SI Appendix*, Table S3). When constraining the shrub data record to 1989 to 2013 in order to match the *P. ponderosa* chronologies, the rate of iWUE increase was 0.89 ± 0.24 μmol CO_2 mol H_2O^{-1} yr^{-1}. These rates of increase greatly exceed those reported in a recent synthesis, which found a global mean increase in forest iWUE of 0.39 μmol CO_2 mol H_2O^{-1} yr^{-1} (6). Indeed, the rate of iWUE increase reported here is 6.9 to 10.3 times greater than the iWUE trend reported across deserts and xeric shrublands in that study, highlighting the atypical nature of such a drastic increase in iWUE in the Southwest. The annual rate of iWUE increase in shrubs was larger than the vast majority of previous estimates in trees (5, 25–28) and to our knowledge is only exceeded by one study of a boreal conifer (29). Vegetation, especially shrublands, in the arid Southwest thus appear to be increasing iWUE at a much faster rate than most regions globally. This increase is especially large in the context of other xeric ecosystems.

Drivers of iWUE Variability Across Plant Functional Types. To uncover the drivers of this abnormally large increase in iWUE, we used a linear mixed effects modeling approach to quantify the sensitivity of iWUE to VPD, PPT, and $[CO_2]$, with a nested random effects structure that included random intercepts and slopes across sites and sample types (i.e., earlywood, latewood, and shrub). Our model explained a large amount of the interannual variability in iWUE (marginal $r^2 = 0.53$, conditional $r^2 = 0.88$). Thus, much of the variability in iWUE was accounted for by the fixed effects (VPD, PPT, and $[CO_2]$), but the inclusion of random effects captured nearly all the variability in iWUE. iWUE was sensitive to fluctuations in VPD, PPT, and $[CO_2]$ (Fig. 3*A*). All else held constant, iWUE was positively related to VPD and $[CO_2]$ and negatively related to PPT, with the exception that PPT was not related to earlywood iWUE (Fig. 4).

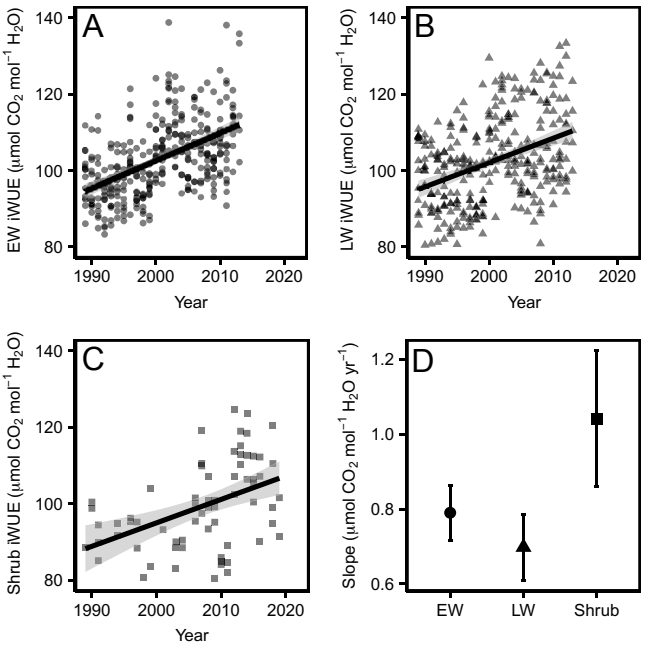

Fig. 2. iWUE has significantly increased over the study period, with the highest rate of increase in shrubs. iWUE in (*A*) earlywood (EW), (*B*) latewood (LW), and (*C*) shrubs, and (*D*) slope parameters of the linear regression for each sample type ± SE. Significant linear relationships ($P < 0.05$) in *A*–*C* are denoted by the presence of a solid linear regression line.

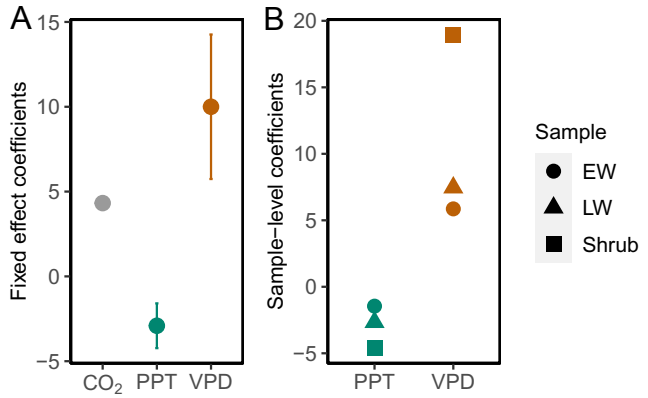

Fig. 3. Sensitivity of iWUE to [CO_2], PPT, and VPD across sample types. (*A*) Fixed effect coefficients with associated SDs, and (*B*) sample-level coefficients for VPD and PPT, for which random slopes were included in the model. Note that the [CO_2] coefficient is not present in *B* because no random slope was included for [CO_2]. EW, earlywood; LW, latewood.

The magnitude of the model coefficient for [CO_2] was larger than that for PPT, indicating that increases in [CO_2] have affected iWUE in the region to a greater degree than PPT. However, the model coefficient for VPD was 3.4 and 2.3 times greater than those for PPT and [CO_2], respectively, highlighting the dominant role of VPD in controlling iWUE. The considerable sensitivity of iWUE to VPD serves as further evidence linking the anomalous increase in iWUE across the Southwest to the ongoing drought.

There are two possible mechanisms for the faster increase in shrub iWUE: more drastic aridification in shrub habitats or a heightened sensitivity of these shrub species to climatic drivers. The mixed model coefficients across sample type indicated that shrub sensitivity to aridity was much greater than *P. ponderosa*, as the VPD coefficient for shrubs was 3.2 and 2.5 times larger than that for earlywood and latewood (respectively) while the PPT coefficient was 2.3 and 1.7 times larger than earlywood and latewood (Fig. 3*B*). The enhanced sensitivity of shrub versus *P. ponderosa* iWUE could potentially arise due to shallower rooting depth among shrubs limiting access to deep stores of moisture that may buffer the leaf-level responses of trees to fluctuations in aridity. If ongoing aridification trends continue, we expect that iWUE will continue to accelerate in these populations irrespective of the growth rate of atmospheric [CO_2]. Likewise, if the Southwest emerges from the megadrought into a relatively wet phase, shrub iWUE may decrease to rates that are more in line with global averages.

The nested random effects structure of the model allowed us to examine cross-site differences in iWUE sensitivity to climatic drivers after accounting for the effects of sample type (*SI Appendix*, Table S4). Site coefficients for VPD were very similar, indicating a fairly uniform leaf-level response to VPD across sites. However, site coefficients for PPT were much more variable, likely since the linkage between PPT and stomatal behavior is more indirect (30), and mediated by factors such as site hydrology, soil properties, and plant root dynamics.

Implications for Plant and Ecosystem Function. Our results have large implications for understanding the interactions between [CO_2] and water availability across plant functional types. First, we demonstrate the powerful impact of long-term drought in accelerating the rise of iWUE. As the increase in iWUE over the past century appears to have slowed down in recent decades (5), water availability could exert increasing control over variability in iWUE given that many regions are expected to experience an intensification of the hydrological cycle (31). In fact, Belmecheri et al. (32) recently documented a surprising stagnation of iWUE in the northeastern United States, attributed to a long-term pluvial period. Second, we show that extrapolating the effects of aridity based solely on tree-ring iWUE may lead to biases in how C and water cycling are changing in regions where nonforested lands are common. More long-term monitoring of various plant functional types or retrospective samplings from herbaria are necessary to uncover these decadal trends in nontree species and constrain existing ecosystem-scale proxies (derived from eddy covariance or remote sensing approaches) for water-use efficiency over nonforested land. To increase our knowledge of the underlying determinants of iWUE, future monitoring efforts should be paired with measurements such as plant allometry, leaf area, and physiology (e.g., hydraulic damage, mesophyll conductance, photosynthetic parameters).

The ultimate impacts of an increase in iWUE on plant physiology, C dynamics, and water use are determined by the degree to which iWUE reflects changes to A versus g_s. Previous syntheses concluded that across more mesic ecosystems, increases in iWUE are largely driven by increases in A (6, 33, 34). However, in arid regions, which are strongly water-limited, it stands to reason that water savings would be prioritized over C gain, and the observed increase in iWUE would be more driven by stomatal closure. Evidence at our sites support this interpretation. Using modeled estimates of *P. ponderosa* leaf water oxygen enrichment ($\Delta^{18}O_{lw}$), we found that 8 out of 13 chronologies significantly increased earlywood $\Delta^{18}O_{lw}$ over the study period while 3 sites increased latewood $\Delta^{18}O_{lw}$ (*SI Appendix*, Fig. S2). As $\Delta^{18}O_{lw}$ varies inversely with relative humidity and stomatal closure, it is likely that many of our sites experienced declines in humidity and g_s during the early growing season. Conversely, the large variability in the iWUE trend during the monsoon season [the wet season when latewood is created (35)] may have been driven by the combined influence of increased A and decreased g_s, though this interpretation is complicated by monsoon-driven increases in humidity that could have decreased evaporative enrichment regardless of g_s. While we lack $\delta^{18}O$ data for shrub foliage, shrub foliar nitrogen [a proxy for photosynthetic rate (36)] has not increased over the study period (37). Coupled with the extreme aridity of the Mojave Desert region, it seems likely that reductions in g_s are driving a large portion of the shrub iWUE trend.

The changes in iWUE documented here and differential sensitivity among functional groups are important for understanding the responses of C and water cycling to increasing [CO_2] and aridity. These global change drivers also impact ecosystems through alterations in plant demography and ecosystem structure. Indeed, drought-induced mortality events in the Southwest have struck the region's forests and woodlands in recent decades (15, 17, 38–40), and wildfires have become more widespread and severe due to the rise in VPD (41). In the case of shrub-dominated ecosystems, this anomalous drought event has coincided with sporadic mass dieback events (18), decreases in recruitment, and shifts to larger and fewer plants (16, 42). While there are ongoing concerns that many dryland ecosystems may be nearing a tipping point (43, 44), the rapid increases in iWUE that we observed have the potential to partially mitigate the impacts of aridification through water savings. The fate of these ecosystems will thus likely rest on the limits of plant acclimation and the future trajectory of this long-term drought event.

Materials and Methods

Sites. Long-term records of iWUE were collected across 16 sites in the American Southwest (Fig. 1*A* and *SI Appendix*, Table S1). Thirteen of these sites consisted of montane *P. ponderosa* stands at the arid end of its range, spread across Colorado, New Mexico, Utah, and Arizona. Three of these sites consisted of various populations of Mojave Desert shrubs: two *Encelia farinosa*

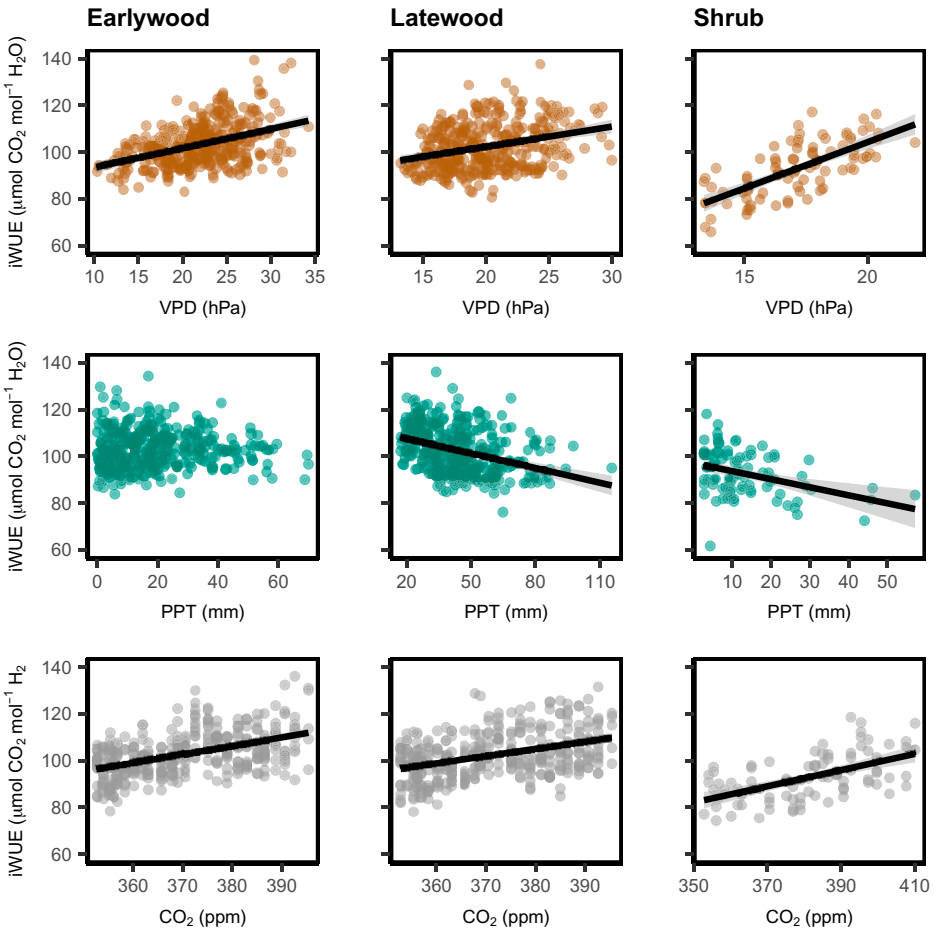

Fig. 4. Primary drivers of iWUE variability. Effects plots showing the relationships between iWUE and VPD, PPT, and [CO_2] across sample types, with the other two variables held constant (i.e., at their mean). Significant relationships ($P < 0.05$) are denoted by the presence of a solid line.

sites in Arizona and southern California and one California site consisting of both *Encelia frutescens* and *Ambrosia salsola*. All sites were near-monospecific for their respective species and are within the spatial extent of the ongoing megadrought (11).

Sample Collection. Shrubs in the *E. farinosa*, *E. frutescens*, and *A. salsola* populations have been surveyed annually from 1989 to 2019 in plots ranging in size from 315 to 450 m^2 (with the exception for dry years when leaves were not present). *E. farinosa* populations have been sampled 29 times over the 31-y study period, while the *E. frutescens* and *A. salsola* populations have been sampled 19 times over the 31-y study period. Annually during the last 2 wk in March, 5 to 10 sunlit leaf samples from the most recent leaf flush for every adult were collected. Since these plants are drought deciduous, these foliar samples primarily reflect C assimilated in the past year. For detailed plot setup and sampling information, see Refs. 24 and 42.

$\delta^{13}C$ and $\delta^{18}O$ isotope chronologies were developed at the *P. ponderosa* stands by sampling cores with a 5 mm increment borer from 4 to 5 trees per site. Sites were selected so as to avoid large watersheds that would influence subsurface hydrology, with no evidence of recent disturbance, and a partially open canopy so as to reduce light competition. All trees selected for coring were medium-aged (100 to 150 y) and fast growing with a well-formed and symmetrical crown. Following sampling, cores were visually cross-dated using standard dendrochronological methods (45). Each tree ring was then sectioned into earlywood and latewood based on changes in color and tracheid density. While these chronologies extend back to the mid-1900s, in this study we largely only consider the rings from 1989 onward to be comparable with the shrub foliar sample record. Plants at all sites were largely fully sunlit, though we cannot rule out the possibility that an increased proportion of shaded needles at *P. ponderosa* sites could dampen the magnitude of iWUE.

Isotope Analysis. Shrub foliar samples were dried after collection and stored in a dark, cool, dry place until analysis. Samples were then ground and analyzed for $\delta^{13}C$ at the Stable Isotope Ratio Facility for Environmental Research at the University of Utah on a Carlo-Erba EA-1110 elemental analyzer coupled with a Finnigan-MAT Delta+ isotope ratio mass spectrometer. Reference materials were calibrated using international standards USGS40 ($\delta^{13}C = -26.24‰$) and USGS41 ($\delta^{13}C = 37.76‰$), and all results are reported in delta notation on the Vienna Pee Dee Belemnite (VPDB) scale. Measurement uncertainty from quality control samples was ± 0.2‰ (SD). Annual population-level mean $\delta^{13}C$ was used for all analyses.

Tree-ring samples were ground and α-cellulose was extracted using a modification of the method of Leavitt and Danzer (46), as described in Szejner et al. (47). Extracted α-cellulose samples were analyzed for $\delta^{13}C$ at the Environmental Isotope Laboratory at the University of Arizona on a high temperature conversion elemental analyzer coupled with a Thermo Delta isotope ratio mass spectrometer. $\delta^{18}O$ was measured on the CO produced by α-cellulose combustion at the Stable Isotope Ratio Facility for Environmental Research at the University of Utah on a Finnigan-MAT Delta+ isotope ratio mass spectrometer. Reference materials were calibrated using international standards IAEA601 ($\delta^{18}O$ = 23.14‰) and IAEA602 ($\delta^{18}O$ = 71.28‰), and all results are reported in delta notation on the Vienna Standard Mean Ocean Water (VSMOW) scale. Measurement uncertainty from quality control samples was ± 0.09‰ SD for $\delta^{13}C$ and ± 0.23‰ for $\delta^{18}O$. Isotope chronologies for each site were constructed by pooling all samples for each year at each site (see Refs. 47 and 48 for more detail regarding chronology construction).

Calculation of iWUE and Leaf Water $\delta^{18}O$. iWUE is determined by the atmospheric CO_2 concentration and the ratio of atmospheric [CO_2] to intracellular [CO_2] (c_i/c_a) (49, 50):

$$iWUE = \frac{A}{g_s} = \frac{c_a\left(1 - \frac{c_i}{c_a}\right)}{1.6}.$$

c_i/c_a is estimated from

$$\delta^{13}C_{plant} = \delta^{13}C_{atm} - a - (b - a)\left(\frac{c_i}{c_a}\right),$$

where $\delta^{13}C_{plant}$ is the foliar or cellulosic isotope ratio, $\delta^{13}C_{atm}$ is isotopic ratio of atmospheric CO_2, and a and b are fractionations associated with CO_2 diffusion (4.4‰) and net carboxylase discrimination (27‰), respectively. We took the additional step of subtracting 2‰ from tree-ring α-cellulose $\delta^{13}C$ to account for known postphotosynthetic fractionations that occur between leaf organic matter and wood α-cellulose (51, 52) and thus make our shrub versus tree estimates of iWUE more comparable in magnitude. Global atmospheric $\delta^{13}C$ and $[CO_2]$ data were obtained from McCarroll and Loader (53), and annual values past 2003 were extrapolated from those data using linear regressions between year and both $\delta^{13}C$ and $[CO_2]$ (6) ($r^2 = 0.99$). $\delta^{13}C_{plant}$ is affected by mesophyll conductance, which is not considered in the traditional linear approach for calculating (c_i/c_a). An alternative approach to calculate iWUE that takes mesophyll conductance into account has been developed (54), though this method requires photosynthetic parameters that have not been measured on our species. While this method tends to slightly increase the magnitude of the temporal iWUE trend when temperature and VPD are increasing over time, we rely on the traditional linear approach for calculating (c_i/c_a) in order to maximize comparability with the existing literature but note that temporal trends in iWUE may differ if alternative approaches are considered.

The $\Delta^{18}O$ of leaf water ($\Delta^{18}O_{lw}$, the enrichment of leaf water $\delta^{18}O$ above source water) allows us to quantify if increases in iWUE are due to constant or decreasing g_s (implying increases in A, inferred through constant or decreasing $\Delta^{18}O_{lw}$ over time) or decreasing g_s (inferred through increasing $\Delta^{18}O_{lw}$ over time). In traditional leaf water enrichment models, relative humidity exerts much more direct control over Δ^{18}Olw than g_s. However, atmospheric aridity and g_s are strongly coupled (55), and this framework thus assumes that g_s-driven trends in Δ^{18}Olw are reflective of both these direct and indirect causes. First, we modeled tree ring α-cellulose $\Delta^{18}O$ as follows:

$$\Delta^{18}O_{plant} = \frac{\delta^{18}O_{plant} - \delta^{18}O_{ppt}}{1 + \left(\frac{\delta^{18}O_{ppt}}{1,000}\right)},$$

where $\delta^{18}O_{plant}$ is the measured cellulosic oxygen isotope ratio and $\delta^{18}O_{ppt}$ is the oxygen isotope ratio of source water, here assumed to be equal to that of precipitation. Annual mean precipitation $\delta^{18}O$ for each site was obtained through simulations from the Isotopes-incorporated Global Spectral Model (56) following the removal of monthly outliers. For earlywood, we used a mean $\delta^{18}O_{ppt}$ from December to May, as this is the period that coincides with winter and spring precipitation at these sites. For latewood, we used a mean $\delta^{18}O_{ppt}$ from July to September to capture the influence of precipitation from the North American Monsoon, which is the primary moisture source that drives latewood growth (46). We then modeled $\Delta^{18}O_{lw}$ as follows (57, 58):

$$\Delta^{18}O_{lw} = \frac{\Delta^{18}O_{plant} - \varepsilon_{wc}}{1 - p_x p_{ex}},$$

where ε_{wc} is a temperature-dependent fractionation (calculated here at 10 °C) during oxygen exchange with water during cellulose synthesis (59), p_x is the fraction of water at the exchange site that is exchangeable (assumed to be 1), and p_{ex} is the fraction of oxygen atoms that are exchanged with water. While p_{ex} is known to vary between species and over time (60–62), we used a value of 0.42 for p_{ex} as it is representative of the mean value for *P. ponderosa* (62). Additionally, our model makes an assumption that precipitation and source water $\delta^{18}O$ are the same, since this approach has been successful in our species and at our sites (48, 63). While these model choices may affect the magnitude of $\Delta^{18}O_{lw}$, a recent sensitivity analysis found that different model choices regarding source water $\delta^{18}O$ have minimal impacts on the temporal trends of $\Delta^{18}O_{lw}$ (6).

Climate Data. Monthly means of precipitation (PPT) were obtained for all sites from the TerraClimate dataset (64), while monthly mean maximum VPD was obtained for all sites from the 4 km PRISM data product (https://prism.oregonstate.edu/). For site PF1, the grid cell containing the nearby town of Shoshone, CA, was used instead since the presence of a weather station greatly improved data quality (24). The PRISM maximum VPD product was used instead of the mean TerraClimate VPD product since maximum VPD reflected variability in iWUE much better across our sites (as evidenced by a fivefold larger correlation coefficient between maximum VPD and iWUE compared with mean VPD and iWUE). The TerraClimate PPT product was used, as its validation error tends to be lower across the Southwest. Model coefficients were similar when run with either PRISM or TerraClimate data (*SI Appendix*, Fig. S3), with slight differences in aridity coefficients due to the stronger relationship between iWUE and maximum VPD than mean VPD.

We aggregated these climate data using different time frames for each sample type (i.e., shrub, earlywood, and latewood) in order to capture the climate window most relevant for plant iWUE. The end of this time frame was determined as the sampling time (for shrub sites) or wood formation time (for tree sites) based on previously published studies at these sites (24, 47). The length of the aggregation window preceding this point was determined by correlating iWUE with mean PPT and maximum VPD across past time frames ranging from 1 mo to 1 y. The time frame that resulted in the maximum sum of statistically significant r^2 values across all sites for a given sample type was chosen. This analysis resulted in optimal climate windows of December to March for shrub samples, May to June for earlywood, and April to September for latewood. Means of monthly PPT and maximum VPD during this period were used in all subsequent analysis.

Statistical Analysis. We used a linear mixed effects model to quantify the sensitivity of shrub versus tree iWUE to climate variability over the past three decades. We focused on three primary drivers of iWUE: atmospheric $[CO_2]$, VPD, and PPT. Both VPD and PPT were used in our model since they capture different facets of water availability (atmospheric aridity versus soil moisture) and were not strongly related in our aggregated climate data ($r^2 = 0.08$). VPD, PPT, and $[CO_2]$ values were centered and scaled (i.e., z-scored) and included as fixed effects. Our model included random effects for site nested within sample type, including random intercepts and random slopes for VPD and PPT. Including a nested random effect for $[CO_2]$ did not alter the model coefficients significantly and resulted in a larger Akaike information criterion. We implemented our model in the R package *lme4* (65) and visually assessed normality and homoscedasticity of residuals (*SI Appendix*, Fig. S4). All model coefficients are reported in *SI Appendix*, Table S4.

There is no consensus regarding best practices for directly quantifying error associated with group-level coefficients in mixed effects models, which incorporate error from both the fixed and random effects. We report the SDs of the conditional modes (*SI Appendix*, Fig. S5 and Table S5) and the error associated with the fixed effects (Fig. 3), which together offer an indication of variance in group-level coefficients. Marginal and conditional r^2 were obtained for our model via the *r.squaredGLMM* function in the R package *MuMIn* (66).

To visualize the effects of climate and CO_2 on iWUE for each sample type, we fit multiple linear regressions including CO_2, PPT, and VPD for earlywood, latewood, and shrub samples separately. Effects plots were created based on this model using the R package *effects* (67), which show the marginal influence of each explanatory variable while the other two explanatory variables are held constant at their mean (i.e., CO_2 and PPT were held constant for the effects plot of VPD). All analyses were done in R 4.0 (68).

Data Availability. All data are available in Dataset S1, including climate, CO_2 concentration, $\delta^{13}C$, and iWUE values. All study data are included in the article and/or supporting information.

ACKNOWLEDGMENTS. Funding for data collection and processing was provided by the NSF Division of Environmental Biology (DEB) grants #1950025 and #1754430. S.A.K. was supported by the NSF DEB Grant #1753845, the US Department of Agriculture (USDA) Forest Service Forest Health Protection Evaluation Monitoring program Grant #19-05, and the US Department of Energy Environmental System Science program Grant #DOE DE-SC0022052. A.W.D. was supported by the NSF DEB Grant #1950025. W.R.L.A. was supported by the David and Lucille Packard Foundation, NSF DEB grants #1714972, #1802880, and #2003017, and USDA National Institute of Food and Agriculture, Agricultural and Food Research Initiative Competitive Program, Ecosystem Services and Agro-Ecosystem Management Grant 2018-67019-27850. This work would not have been possible without the numerous individuals involved in annual shrub surveys, and we thank them immensely. We would also like to thank Mickey Campbell for assistance with mapping land cover.

1. J. A. Berry, D. J. Beerling, P. J. Franks, Stomata: Key players in the earth system, past and present. *Curr. Opin. Plant Biol.* **13**, 233–240 (2010).
2. C. Field, R. Jackson, H. Mooney, Stomatal responses to increased CO_2: Implications from the plant to global scale. *Plant Cell Environ.* **18**, 1212–1225 (1995).
3. L. Lemordant, P. Gentine, A. S. Swann, B. I. Cook, J. Scheff, Critical impact of vegetation physiology on the continental hydrologic cycle in response to increasing CO_2. *Proc. Natl. Acad. Sci. U.S.A.* **115**, 4093–4098 (2018).
4. C. B. Skinner, C. J. Poulsen, R. Chadwick, N. S. Diffenbaugh, R. P. Fiorella, The role of plant CO_2 physiological forcing in shaping future daily-scale precipitation. *J. Clim.* **30**, 2319–2340 (2017).
5. M. A. Adams, T. N. Buckley, T. L. Turnbull, Diminishing CO_2-driven gains in water-use efficiency of global forests. *Nat. Clim. Chang.* **19**, 466–471 (2020).
6. J. M. Mathias, R. B. Thomas, Global tree intrinsic water use efficiency is enhanced by increased atmospheric CO_2 and modulated by climate and plant functional types. *Proc. Natl. Acad. Sci. U.S.A.* **118**, e2014286118 (2021).

7. M. Saurer, R. T. W. Siegwolf, F. H. Schweingruber, Carbon isotope discrimination indicates improving water-use efficiency of trees in northern Eurasia over the last 100 years. *Glob. Change Biol.* **10**, 2109–2120 (2004).
8. W. Peters *et al.*, Increased water-use efficiency and reduced CO_2 uptake by plants during droughts at a continental-scale. *Nat. Geosci.* **11**, 744–748 (2018).
9. Y. Yang *et al.*, Contrasting responses of water use efficiency to drought across global terrestrial ecosystems. *Sci. Rep.* **6**, 23284 (2016).
10. A. Dai, Increasing drought under global warming in observations and models. *Nat. Clim. Chang.* **3**, 52–58 (2013).
11. A. P. Williams *et al.*, Large contribution from anthropogenic warming to an emerging North American megadrought. *Science* **368**, 314–318 (2020).
12. C. R. Schwalm *et al.*, Reduction in carbon uptake during turn of the century drought in western North America. *Nat. Geosci.* **5**, 551–556 (2012).
13. P. Szejner, S. Belmecheri, J. R. Ehleringer, R. K. Monson, Recent increases in drought frequency cause observed multi-year drought legacies in the tree rings of semi-arid forests. *Oecologia* **192**, 241–259 (2020).
14. P. Szejner *et al.*, Stable isotopes of tree rings reveal seasonal-to-decadal patterns during the emergence of a megadrought in the Southwestern US. *Oecologia* **197**, 1079–1094 (2021).
15. D. D. Breshears *et al.*, Regional vegetation die-off in response to global-change-type drought. *Proc. Natl. Acad. Sci. U.S.A.* **102**, 15144–15148 (2005).
16. S. Hantson, T. E. Huxman, S. Kimball, J. T. Randerson, M. L. Goulden, Warming as a driver of vegetation loss in the Sonoran Desert of California. *J. Geophys. Res. Biogeosciences* **126** e2020JG005942 (2021).
17. S. A. Kannenberg, A. W. Driscoll, D. Malesky, W. R. L. Anderegg, Rapid and surprising dieback of Utah juniper in the southwestern USA due to acute drought stress. *For. Ecol. Manage.* **480**, 118639 (2021).
18. J. R. McAuliffe, E. P. Hamerlynck, Perennial plant mortality in the Sonoran and Mojave deserts in response to severe, multi-year drought. *J. Arid Environ.* **74**, 885–896 (2010).
19. E. A. Ainsworth, S. P. Long, What have we learned from 15 years of free-air CO_2 enrichment (FACE)? A meta-analytic review of the responses of photosynthesis, canopy properties and plant production to rising CO_2. *New Phytol.* **165**, 351–371 (2005).
20. B. I. Cook, T. R. Ault, J. E. Smerdon, Unprecedented 21st century drought risk in the American Southwest and Central Plains. *Sci. Adv.* **1**, e1400082 (2015).
21. R. Seager *et al.*, Projections of declining surface-water availability for the southwestern United States. *Nat. Clim. Chang.* **3**, 482–486 (2013).
22. B. Cook *et al.*, Uncertainties, limits, and benefits of climate change mitigation for soil moisture drought in Southwestern North America. Earth's *Future* **9**, e2021EF002014 (2021).
23. M. Rollins, LANDFIRE: A nationally consistent vegetation, wildland fire, and fuel assessmen. *Int. J. Wildland Fire* **18**, 235–249 (2009).
24. A. W. Driscoll, N. Q. Bitter, D. R. Sandquist, J. R. Ehleringer, Multidecadal records of intrinsic water-use efficiency in the desert shrub *Encelia farinosa* reveal strong responses to climate change. *Proc. Natl. Acad. Sci. U.S.A.* **117**, 18161–18168 (2020).
25. M. Lévesque, R. Siegwolf, M. Saurer, B. Eilmann, A. Rigling, Increased water-use efficiency does not lead to enhanced tree growth under xeric and mesic conditions. *New Phytol.* **203**, 94–109 (2014).
26. J. Peñuelas, J. G. Canadell, R. Ogaya, Increased water-use efficiency during the 20th century did not translate into enhanced tree growth. *Glob. Ecol. Biogeogr.* **20**, 597–608 (2011).
27. C. C. Reed, A. P. Ballantyne, L. A. Cooper, A. Sala, Limited evidence for CO_2-related growth enhancement in northern Rocky Mountain lodgepole pine populations across climate gradients. *Glob. Chang. Biol.* **24**, 3922–3937 (2018).
28. P. Van Der Sleen *et al.*, No growth stimulation of tropical trees by 150 years of CO_2 fertilization but water-use efficiency increased. *Nat. Geosci.* **8**, 24–28 (2015).
29. C. Giguère-Croteau *et al.*, North America's oldest boreal trees are more efficient water users due to increased [CO_2], but do not grow faster. *Proc. Natl. Acad. Sci. U.S.A.* **116**, 2749–2754 (2019).
30. T. N. Buckley, Modeling stomatal conductance. *Plant Physiol.* **174**, 572–582 (2017).
31. F. Giorgi *et al.*, Higher hydroclimatic intensity with global warming. *J. Clim.* **24**, 5309–5324 (2011).
32. S. Belmecheri *et al.*, Precipitation alters the CO_2 effect on water-use efficiency of temperate forests. *Glob. Change Biol.* **27**, 1560–1571 (2021).
33. R. Guerrieri *et al.*, Disentangling the role of photosynthesis and stomatal conductance on rising forest water-use efficiency. *Proc. Natl. Acad. Sci. U.S.A.* **116**, 16909–16914 (2019).
34. M. A. Adams, T. N. Buckley, D. Binkley, M. Neumann, T. L. Turnbull, CO_2, nitrogen deposition and a discontinuous climate response drive water use efficiency in global forests. *Nat. Commun.* **12**, 5194 (2021).
35. K. Morino, R. L. Minor, G. A. Barron-Gafford, P. M. Brown, M. K. Hughes, Bimodal cambial activity and false-ring formation in conifers under a monsoon climate. *Tree Physiol.* **41**, 1893–1905 (2021).
36. J. R. Evans, Photosynthesis and nitrogen relationships in leaves of C_3 plants. *Oecologia* **78**, 9–19 (1989).
37. A. W. Driscoll, S. A. Kannenberg, J. R. Ehleringer, Long-term nitrogen isotope dynamics in Encelia farinosa reflect plant demographics and climate. *New Phytol.* **232**, 1226–1237. (2021).
38. W. R. L. Anderegg *et al.*, The roles of hydraulic and carbon stress in a widespread climate-induced forest die-off. *Proc. Natl. Acad. Sci. U.S.A.* **109**, 233–237 (2012).
39. C. J. Fettig, L. A. Mortenson, B. M. Bulaon, P. B. Foulk, Tree mortality following drought in the central and southern Sierra Nevada, California, U.S. *For. Ecol. Manage.* **432**, 164–178 (2019).
40. J. L. Ganey, S. C. Vojta, Tree mortality in drought-stressed mixed-conifer and ponderosa pine forests, Arizona, USA. *For. Ecol. Manage.* **261**, 162–168 (2011).
41. J. T. Abatzoglou, A. P. Williams, Impact of anthropogenic climate change on wildfire across western US forests. *Proc. Natl. Acad. Sci. U.S.A.* **113**, 11770–11775 (2016).
42. J. R. Ehleringer, D. R. Sandquist, A tale of ENSO, PDO, and increasing aridity impacts on drought-deciduous shrubs in the Death Valley region. *Oecologia* **187**, 879–895 (2018).
43. B. T. Bestelmeyer *et al.*, Desertification, land use, and the transformation of global drylands. *Front. Ecol. Environ.* **13**, 28–36 (2015).
44. D. L. Hoover *et al.*, Traversing the Wasteland: A Framework for Assessing Ecological Threats to Drylands. *Bioscience* **70**, 35–47 (2020).
45. M. A. Stokes, T. L. Smiley, *An Introduction to Tree-Ring Dating* (University of Arizona Press, Tucson, AZ, 1999).
46. S. W. Leavitt, S. R. Danzer, Method for batch processing small wood samples to holocellulose for stable-carbon isotope analysis. *Anal. Chem.* **65**, 87–89 (1993).
47. P. Szejner *et al.*, Latitudinal gradients in tree ring stable carbon and oxygen isotopes reveal differential climate influences of the North American Monsoon System. *J. Geophys. Res. Biogeosci.* **121**, 1978–1991 (2016).
48. P. Szejner *et al.*, Disentangling seasonal and interannual legacies from inferred patterns of forest water and carbon cycling using tree-ring stable isotopes. *Glob. Chang. Biol.* **24**, 5332–5347 (2018).
49. G. Farquhar, M. O'Leary, J. Berry, On the relationship between carbon isotope discrimination and the intercellular carbon dioxide concentration in leaves. *Aust. J. Plant Physiol.* **9**, 121–137 (1982).
50. G. Farquhar, J. Ehleringer, K. Hubick, Carbon isotope discrimination and photosynthesis. *Annu. Rev. Plant Physiol. Plant Mol. Biol.* **40**, 503–537 (1989).
51. F. W. Badeck, G. Tcherkez, S. Nogués, C. Piel, J. Ghashghaie, Post-photosynthetic fractionation of stable carbon isotopes between plant organs—A widespread phenomenon. *Rapid Commun. Mass Spectrom.* **19**, 1381–1391 (2005).
52. L. A. Cernusak *et al.*, Why are non-photosynthetic tissues generally ^{13}C enriched compared with leaves in C_3 plants? Review and synthesis of current hypotheses. *Funct. Plant Biol.* **36**, 199–213 (2009).
53. D. McCarroll, N. J. Loader, Stable isotopes in tree rings. *Quat. Sci. Rev.* **23**, 771–801 (2004).
54. U. Seibt, A. Rajabi, H. Griffiths, J. A. Berry, Carbon isotopes and water use efficiency: Sense and sensitivity. *Oecologia* **155**, 441–454 (2008).
55. C. Grossiord *et al.*, Plant responses to rising vapor pressure deficit. *New Phytol.* **226**, 1550–1566 (2020).
56. K. Yoshimura, M. Kanamitsu, D. Noone, T. Oki, Historical isotope simulation using Reanalysis atmospheric data. *J. Geophys. Res. Atmos.* **113**, D19108 (2008).
57. M. M. Barbour, Stable oxygen isotope composition of plant tissue: A review. *Funct. Plant Biol.* **34**, 83–94 (2007).
58. A. W. Cheesman, L. A. Cernusak, Infidelity in the outback: Climate signal recorded in Δ18O of leaf but not branch cellulose of eucalypts across an Australian aridity gradient. *Tree Physiol.* **37**, 554–564 (2017).
59. L. Sternberg, P. F. V. Ellsworth, Divergent biochemical fractionation, not convergent temperature, explains cellulose oxygen isotope enrichment across latitudes. *PLoS One* **6**, e28040 (2011).
60. A. Gessler *et al.*, Tracing carbon and oxygen isotope signals from newly assimilated sugars in the leaves to the tree-ring archive. *Plant Cell Environ.* **32**, 780–795 (2009).
61. A. Gessler *et al.*, The oxygen isotope enrichment of leaf-exported assimilates—does it always reflect lamina leaf water enrichment? *New Phytol.* **200**, 144–157 (2013).
62. P. Szejner, T. Clute, E. Anderson, M. N. Evans, J. Hu, Reduction in lumen area is associated with the δ^{18} O exchange between sugars and source water during cellulose synthesis. *New Phytol.* **226**, 1583–1593 (2020).
63. S. Belmecheri, W. E. Wright, P. Szejner, K. A. Morino, R. K. Monson, Carbon and oxygen isotope fractionations in tree rings reveal interactions between cambial phenology and seasonal climate. *Plant Cell Environ.* **41**, 2758–2772 (2018).
64. J. T. Abatzoglou, S. Z. Dobrowski, S. A. Parks, K. C. Hegewisch, TerraClimate, a high-resolution global dataset of monthly climate and climatic water balance from 1958-2015. *Sci. Data* **5**, 170191 (2018).
65. D. Bates, M. Mächler, B. Bolker, S. Walker, Fitting linear mixed-effects models using lme4. *J. Stat. Softw.* **67**, 1–48 (2015).
66. K. Barton, MuMIn: Multi-Model Inference. R package version 1.43.17. https://cran.r-project.org/web/packages/MuMIn/index.html. Accessed 17 July 2021.
67. J. Fox, S. Weisberg, *An R Companion to Applied Regression* (SAGE Publications, Inc, Thousand Oaks, CA, ed. 3, 2019).
68. R Core Team, *R: A Language and Environment for Statistical Computing* (R Foundation for Statistical Computing, Vienna, Austria, 2021).